Structure-Function Insights into Thermoresponsive Copolymers as Lanthanide Precipitants

Supraja S. Chittari, Peter A. Dykeman-Bermingham, Matthew P. Bogen, Abigail S. Knight

Abstract

The synthetic toolbox for stimuli-responsive polymers has broadened to include many variables of tunable control, making these materials applicable in diverse technologies. However, unraveling the key composition-structure-function relationships to facilitate ground-up design remains a challenge due to the inherent dispersity in sequence and conformations for synthetic polymers. We here present a systematic study of these relationships using a model system of copolymers with a thermoresponsive (*N*-isopropylacrylamide) backbone in addition to metal-chelating (acrylic acid) and hydrophobic structural comonomers and evaluate their efficiency at the isolation of technologically critical lanthanide ions. The efficiency of lanthanide ion extraction by precipitation was quantitated with a metallochromic dye to reveal trends relating copolymer hydrophobicity to improved separations. Further, we examined the role of different hydrophobic comonomers in dictating solution-phase conformation of the polymer in the presence and absence of lanthanide ions, and we identify key features of the hydrophobic comonomer that influence extraction efficiency. Finally, we identified how the local proximity of thermoresponsive, chelating, and hydrophobic subunits facilitate metal extraction by manipulating copolymer sequence with multiblock polymerization. Through mechanistic analysis, we propose a binding-then-assembly process through which metal ions are coprecipitated with macromolecular chelators.

Introduction

The versatility and modularity of synthetic polymers have led to their application in diverse technologies, from chemical separations[1] to protein stabilization.[2] As the suite of synthetic tools for polymer synthesis has expanded, strategies have been developed to control the monomer patterning with multiblock copolymers[3] and elements of protein-like hierarchical structure, yielding materials with complex functions including binding to target species[4,5] and catalysis.[6,7] However, connecting macromolecule composition and patterning to desired conformational and functional outcomes remains a significant challenge. Much like intrinsically disordered proteins offer both stimuli-responsive and phase separation capabilities,[8] dynamic solution-phase copolymers may be leveraged for complex functions, particularly in industrial separations that can uniquely benefit from stimuli-responsive behavior.[9] For example, polymers with thermoresponsive backbones have been designed for solid-liquid separations such isolating minerals (e.g., silica or alumina) from suspensions[10,11] and the purification of proteins (e.g., immunoglobulin G or human serum albumin) by high-affinity binding.[12,13] However, much of this work involves immobilization of stimuli-responsive materials on solid supports such as membranes,[14] hydrogels,[15] or beads.[16] In these environments, features of the hierarchical structure of these polymers, which are inherently intertwined with their function, cannot be fully explored. Therefore, further elucidation of

underlying structure-function relationships will enhance our ability to harness the potential of responsive synthetic copolymers.

To probe fundamental structure-function principles to guide the design of responsive copolymers, we investigated lanthanide binding as a model system. The isolation and separation of rare-earth elements, particularly lanthanide ions, is of critical importance to meet demands in technological development and currently presents a challenge due to similarities in ionic radius and coordination number.[17] Common industrial strategies including solvent extraction[18,19] and ion-exchange chromatography,[20,21] are time-, resource-, and cost-intensive, motivating efforts to discover alternative or augmented methods. Amongst these alternatives, the design of novel bio-inspired polymers has been used to tune the affinity and selectivity of lanthanide binding by conferring hierarchical structure.[22] For example, the unstructured lanthanide ion mineralization peptide (Lamp), discovered through phage display screening, was demonstrated to bind and precipitate heavy lanthanide ions over light ions and represents an avenue to energy-inexpensive separations method.[23] Drawing inspiration from these efforts, we sought to identify structure-property relationships for analogous polymeric metal precipitants that offer both enhanced scalability and chemical tunability. Polymer composition,[24] tacticity,[25] and monomer patterning[26] have been demonstrated to impact in-solution affinity for lanthanide ions, but design principles defining the relationship between polymer properties and efficient and selective precipitants remain limited. Through the systematic variation of the composition and monomer patterning of thermoresponsive copolymers, herein we identify connections between copolymer composition, solution structure, and separation ability for lanthanide (III) ions in an environmentally benign aqueous environment, providing fundamental insights towards the design of desirable synthetic sequestrants.

Results and Discussion

Characterization of the Impact of Copolymer Hydrophobicity on Lanthanide Extraction

To target responsive polymers capable of phase separation upon binding lanthanide (III) (Ln^{3+}) ions in a benign aqueous environment, we designed copolymers on the fringes of aqueous solubility through selection of three categories of comonomers: thermoresponsive, structural, and metal-chelating. Rapid and often reversible control of polymer phase behavior through temperature modulation have already made thermoresponsive polymers attractive in sensing[27] and separations[28] applications. Therefore, we chose poly(*N*-isopropylacrylamide) (pNIPAM) as a thermoresponsive backbone because of its lower critical solution temperature (LCST) close to ambient conditions (~32 °C).[29] The addition of hydrophobic structural monomers has been shown to modulate physical properties of thermoresponsive polymers, such as reduction of cloud point temperatures[30] and increases in the sizes of self-assembled morphologies.[31] In contrast, the addition of hydrophilic and charged residues, such as acrylic acid (AA), copolymerized with pNIPAM has been shown to have the opposite effect thermal behavior by increasing the cloud point.[32–34] In addition to their effect on cloud point, charged monomers like AA in their carboxylate

form are capable of metal-binding[35,36] (e.g., chelation of heavy metal ions[37–39]). As previous work has focused predominantly on solid-phase extractants, such as hydrogels,[15] and functionalized solid supports, such as magnetic beads,[38] design principles connecting polymer structure to ion affinity and selectivity remain limited. Therefore, this three-monomer model system containing thermoresponsive, hydrophobic, and binding units offers a rich thermodynamic landscape and many synthetic degrees of freedom through which to investigate relationships between copolymer composition, structure, and function as lanthanide precipitants (Figure 1a).

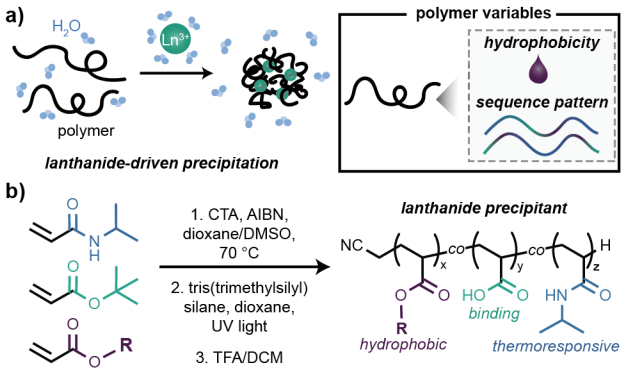

Figure 1. Thermoresponsive library design. (a) Schematic of polymeric precipitants, with key variables including copolymer hydrophobicity and sequence patterning. (b) General overview of synthesis of *N*-isopropylacrylamide (NIPAM) statistical copolymers with a pro-functional monomer (*tert*-butyl acrylate, *t*BA) and a hydrophobic acrylate comonomer. Polymerization was performed using a chain transfer agent (CTA) and azobisisobutyronitrile (AIBN) as an initiator in a mixture of 1,4-dioxane and dimethyl sulfoxide (DMSO) as solvents. Polymerization was followed by capping of the chain end with tris(trimethylsilyl) silane (TTMSS) and deprotection of *t*BA using a mixture of trifluoroacetic acid (TFA) in dichloromethane (DCM) to reveal the carboxylate side chain.

We synthesized a series of thermoresponsive, metal-binding copolymers in a three-step scheme (Figure 1b). A series of model copolymers were synthesized with increasing mole percents of a hydrophobic monomer, butyl acrylate (BA) [**P1-BA(5)**, **P2-BA(10)**, and **P3-BA(15)**; Figure 2a, left]. These statistical copolymers were synthesized with reversible addition-fragmentation chain transfer (RAFT) polymerization in 1,4-dioxane/DMSO to access controlled molecular weights and low dispersities (Đ < 1.1; Table 1, Figure S1-7).[40] A target molecular weight of ~10 kDa was selected as PNIPAM homopolymers at this molecular weight exhibit a cloud point close to 32 °C, just above room temperature.[29,41] For each copolymer, the incorporation of AA was fixed at 25 mol % to ensure that the majority of the polymer backbone was comprised of structural and thermoresponsive monomers that fine tune the phase separation behavior. An AA-precursor monomer, *tert*-butyl acrylate (*t*BA),[42] was selected as it demonstrated a monomer incorporation rate closer to that of NIPAM than the rate displayed by acrylic acid under the same conditions

(Figure S8). As polymer chain ends have been shown to impact self-assembly processes,[43,44] we removed the terminal trithiocarbonate using tris(trimethylsilyl) silane as a proton capping agent under UV light (Figure S9).[45] Finally, the *t*BA group was cleaved under acidic conditions (trifluoroacetic acid in DCM) to reveal the AA moiety.[46] Successful chain end capping and removal of *t*BA were confirmed by ^{1}H NMR (Figure S10-12).

polymer label	hydrophobic monomer (mol %)	hydrophobic monomer (wt %)	AA (mol %)	MW (kDa)	$Đ_{DMF}$
P1-BA(5)	5 % BA	6 % BA	23	11.3	1.09
P2-BA(10)	10 % BA	12 % BA	24	10.4	1.06
P3-BA(15)	15 % BA	18 % BA	25	10.7	1.07
P4-*i*BA	5 % isoBA	6 % isoBA	24	9.9	1.07
P5-*c*HA	4 % cHA	7 % cHA	24	10.2	1.07
P6-HA	4 % HA	7 % HA	25	10.2	1.07
P7-IBOA	3 % iBOA	6 % iBOA	25	10.1	1.09
P8-LA	3 % LA	7 % LA	25	10.2	1.08
b1	9 % BA	11 % BA	23	12.9	1.13
b2	10 % BA	12 % BA	24	13.8	1.13
stat	9 % BA	11 % BA	22	13.1	1.09

Table 1. ^{1}H and DMF SEC characterization of copolymers. Monomer abbreviations: butyl acrylate (BA), *iso*-butyl acrylate (*i*BA), cyclohexyl acrylate (*c*HA), hexyl acrylate (HA), isobornyl acrylate (IBOA), lauryl acrylate (LA), and acrylic acid (AA). Molecular weight was calculated from ^{1}H NMR. DMF SEC characterization is of copolymers after chain-end capping but prior to *t*BA deprotection due to compatibility with DMF SEC characterization.

Precipitation of the series of model polymers was visually observed upon the chelation of a model lanthanide Eu^{3+} (0.5 mM $EuCl_3$, 40 mM MES, 100 mM KCl, pH 6) at a 3:1 [Eu^{3+}]:[AA] stoichiometry to ensure deprotonation of carboxylate groups. The phase separation was monitored by changes in solution turbidity using a UV-Vis cuvette reader (550 nm detection) (Figure 2b, S13-14). We hypothesized that both temperature and hydrophobicity would modulate the efficiency of phase separation due to strong coupling between these two features in LCST systems. A cloud point was observed in metal-free buffer at high temperatures (> 70 °C) or not observed at all for these copolymers (Figure S15). Thus, a fixed incubation temperature (31 °C) close to cloud point temperature of pNIPAM homopolymers[47] was selected to perform turbidimetry analyses of metal-binding driven aggregation. We observed that solution turbidity increased more rapidly with increasing mol % of the hydrophobic monomer, BA (Figure 1b, left). Further, phase separation was more rapid at with higher temperatures (41 °C and 51 °C) for **P1-BA(5)** (Figure 2b, right).

While increased turbidity is indicative of increased phase separation, we further sought to quantitate the amount of metal coprecipitated with the polymer as a function of polymer hydrophobicity. To achieve this, **P1-BA(5)**, **P2-BA(10)**, and **P3-BA(15)** were incubated with 0.5 mM Eu^{3+} at a ratio of 1 [Eu^{3+}]: 3 [AA] at a range of temperatures (20 – 51 °C) and any aggregates were isolated via centrifugation (Figure 2a, right). The efficiency of lanthanide isolation was determined by comparing the concentration of residual metal in the supernatant to that of the original solution. The supernatant concentration was quantified via complexation to Arsenazo III, a metallochromic indicator for Ln^{3+} practical at low pH values required to protonate carboxylates on any residual polymer in the supernatant (Figure S16).[48] Both increased temperature and hydrophobicity improved pulldown efficiency (Figure 2c, left), analogous to the trends observed for phase separation. Further, both **P2-BA(10)** and **P3-BA(15)** isolated > 90% of the Eu^{3+} in an aqueous solution within this mild temperature range.

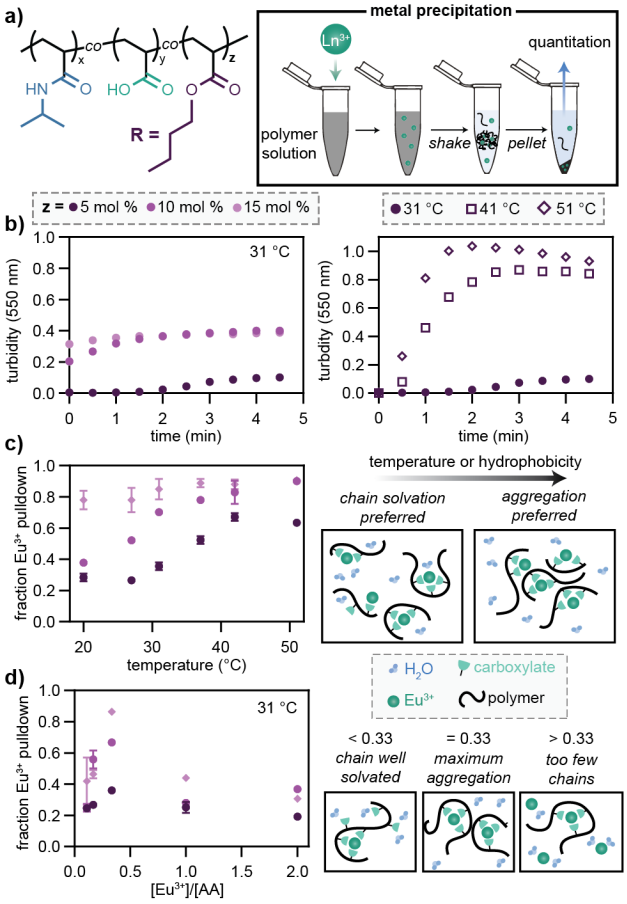

Figure 2. Comparisons of model copolymers with varied mol % butyl acrylate (BA) for Eu^{3+} isolation. (a) (left) Schematic of copolymers synthesized at 5, 10 and 15 mol % BA. (right) Cartoon describing the metal precipitation assay with quantitation via a metallochromic dye. (b) Turbidimetry measurements at 550 nm of (left) increasing mol % BA copolymers [**P1-BA(5)**, **P2-BA(10)**, **P3-BA(15)**]

incubated at 31 °C and (right) a 5 mol % BA copolymer [**P1-BA(5)**] incubated at 31, 41, and 51 °C. (c) Eu^{3+} isolation quantitated for increasing mol % BA copolymers [**P1-BA(5)**, **P2-BA(10)**, **P3-BA(15)**] at increasing incubation temperatures (n = 3, error bars represent standard deviation). Schematic representing increasing aggregation driven by increasing chain hydrophobicity. (d) Eu^{3+} isolation quantitated for increasing mol % BA copolymers [**P1-BA(5)**, **P2-BA(10)**, **P3-BA(15)**] at changing stoichiometry of [Eu^{3+}]:[AA] (n = 3, errors represent standard deviation). Schematic representing a hypothesized stoichiometric dependence of pulldown.

Observations from both turbidimetry analysis and the metal extraction assay may be attributed to the impact of polymer hydrophobicity on intermolecular interactions (Figure 2c, right). At increased mol % BA, the increased hydrophobicity of the backbone drives aggregation, resulting in increased Eu^{3+} extraction efficiency and more rapid aggregation at a fixed temperature. Increased copolymer hydrophobicity has also been shown to shift distributions to larger aggregate sizes and improve performance as flocculants.[49] However, a similar behavior can be achieved even at fixed mol % BA as increasing the temperature increases the hydrophobicity of the NIPAM backbone, characteristic of LCST transitions.[28]

The selection of the ratio of ion (Ln^{3+}) to ligand (AA) of 1:3 was initially based on charge neutrality, although decreasing the molar ratio of [Ln^{3+}]:[AA] has been shown to decrease the metal adsorption of poly(acrylic acid) to Ce^{3+}.[50] To investigate analogous stoichiometric effects on polymer-metal precipitation, we fixed the concentration of Eu^{3+} at 0.5 mM and varied the concentration of each copolymer to achieve six ratios of [Eu^{3+}]/[AA]. After incubation and removal of polymer aggregates, we measured the fraction of Eu^{3+} remaining in the supernatant. For each copolymer tested, a maximum was observed at [Eu^{3+}]/[AA] = 0.33 (Figure 2d, left). Similar optimization of aggregation at charge neutrality was also described in chemo- and biosensing polyelectrolytes.[51] We hypothesize that below this ratio, chelating groups are in excess and aid in solvating the chain, preventing interchain association (Figure 2d, right). At a 1:3 ratio of metal to AA units, most chelating groups are engaged in binding due to charge equivalence, driving chain association. Finally, above this ratio, metal ions are in excess, and chains are too few to assemble.

Motivated by the strong coupling between chain hydrophobicity and efficiency of lanthanide isolation, we synthesized a set of copolymers with additional hydrophobic pendent side chains to deconvolute effects of both alkyl side chain length and architecture. Two four-carbon [*n*-butyl acrylate (BA) and *iso*-butyl acrylate (*i*BA)), six-carbon (*n*-hexyl acrylate (HA) and cyclohexyl acrylate (*c*HA)], ten-carbon [isobornyl acrylate (IBOA)], and twelve-carbon [lauryl acrylate (LA)] comonomers were chosen and copolymerized with NIPAM and *t*BA (Figure 3a, S17-27). Copolymers (**P4-*i*BA**, **P5-*c*HA**, **P6-HA**, **P7-IBOA**, **P8-LA**) were synthesized as previously described at similar weight percents of the hydrophobic monomer (~6 wt %) to facilitate

comparisons across similar global hydrophobicities (Figure S28-32). To probe rigidity and in-solution compaction, we initially used small-angle X-ray scattering (SAXS) to probe these structural parameters with a limited subset that could capture effects of both alkyl side chain length and architecture (**P1-BA(5)**, **P6-HA**, **P5-*c*HA**, and **P8-LA)**. The radius of gyration (R_g) describing the chain size and Porod exponent describing chain stiffness were calculated by fitting SAXS scattering profiles of copolymers dissolved at 2.5 mg/mL to the polymer excluded volume model[52] or the Guinier-Porod[53] model which each describe flexible polymer chains (Figure S33, Table S1). This analysis revealed the smallest R_g (29.2 Å) and highest Porod exponent (2.2) for **P8-LA**, where the largest monomer, lauryl acrylate, drives conformationally constrained folding. Projection of the SAXS profiles in a dimensionless Kratky plot allows for a visual assessment of chain compaction normalized for molecular weight and R_g. In this projection, **P8-LA** exhibits a weak inflection point and plateau at $q \bullet R_g = 2$, similar to many intrinsically disordered proteins (IDPs).[54] Further, **P8-LA** is more compact than the other copolymers in this series that show increasing scattering intensity with $q \bullet R_g$ indicative of more chain flexibility (Figure 3b, left).

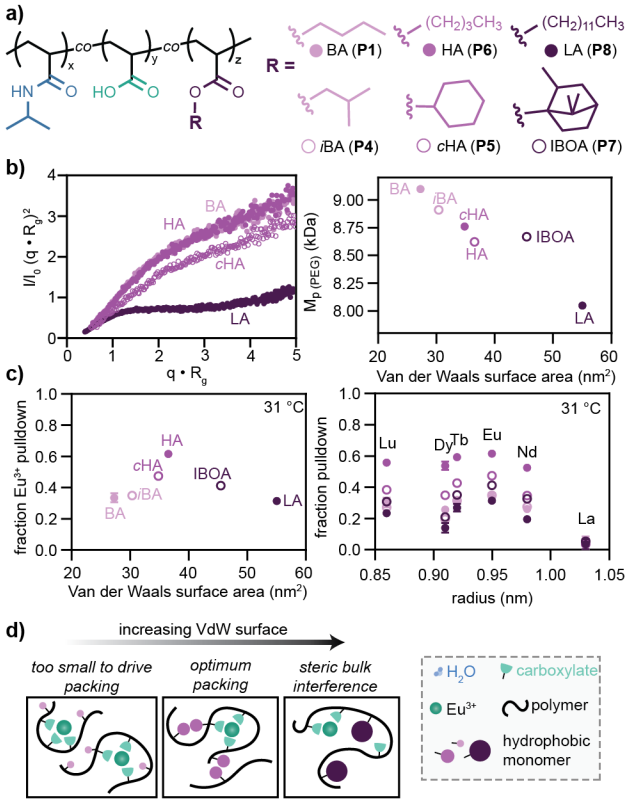

Figure 3. Comparison of copolymers with the same global hydrophobicity. (a) Scope of selected hydrophobic comonomers incorporated to similar wt % in associated statistical copolymers are butyl acrylate [**P1-BA(5)**], *iso*-butyl acrylate (**P4-*i*BA**), cyclohexyl acrylate (**P5-*c*HA**), *n*-hexyl acrylate (**P6-HA**), and isbornyl acrylate (**P7-IBOA**). (b) Solution-phase conformations of copolymers in the absence of metal. (left) Dimensionless Kratky projections of SAXS scattering

profiles for **P1-BA(5)**, **P5-*c*HA**, **P6-HA**, **P8-LA**. (right) $M_{p\ (PEG)}$ of copolymers acquired from PEG standards calibration standards plotted against Van der Waals surface area calculated from DFT simulations. (c) (left) Extraction of Eu^{3+} by copolymers at 31 °C (n = 3, error bars represent standard deviation). (right) Extraction of multiple Ln^{3+} ions (denoted in plot) by copolymers at 31 °C (n = 3, error bars represent standard deviation). (d) Schematic of maximized ion isolation through optimum multichain packing during aggregation.

We further corroborated the relationship between monomer size and solution-phase conformations of the full series of copolymers (unbound to Ln^{3+}) using aqueous size exclusion chromatography (SEC_{aq}; 40 mM MES, 100 mM KCl, pH 6; Figure 3b, right). To quantitatively compare the hydrated size of each copolymer, the molecular weight at the peak maxima as compared to PEG standards ($M_{p\ (PEG)}$) were extracted. As the copolymers were synthesized with similar molecular weights (Figure S27), we hypothesized this measure of compactness could be correlated to chemical descriptors of the hydrophobic comonomer. A series of calculations were performed on each monomer using DFT to identify the significance of different chemical descriptors (Table S2),[55,56] and we identified that the Van der Waals (VdW) surface area strongly correlates with the $M_{p\ (PEG)}$ (Pearson correlation coefficient of -0.94, Figure 3b, right). This correlation demonstrates that increased monomer steric bulk drives chain compaction in the aqueous conditions evaluated. Similar phenomena have also been observed in single-chain folding where increased carbon count and LogP drive increased chain compaction,[57,58] and in multi-chain assembly, where the LogP of comonomers drove an increase in assembly size that required increased surface charge to solubilize.[59] In these cases, as well as the present work, chain collapse may correlate well with descriptors of hydrophobicity such as VdW surface area, LogP, or carbon count.

As this structural analysis was performed with unbound copolymers, we further probed the efficacy of Eu^{3+} isolation for each of the copolymers in this series using centrifugation and dye-based quantification as previously described (Figure 3c, left). The fraction of metal isolated was inconsistent despite the uniform global hydrophobicity of the copolymers. Contrary to the observed polymer collapse, the relationship between the VdW surface area of the hydrophobic comonomer and the fraction pulldown is nonlinear: a peak is observed for hexyl acrylate and the efficiency decays at both larger and smaller surface area comonomers. To determine if this trend is consistent across lanthanide ions with different ionic radii, we expanded our scope to include five additional lanthanide salts (Lu^{3+}, Dy^{3+}, Tb^{3+}, Eu^{3+}, Nd^{3+}, and La^{3+}; Figure 3c, right and Table S3). The **P6-HA** consistently isolated a higher fraction of the ions in solution than the other copolymers. While each copolymer exhibits slightly different extraction efficiency towards different ionic radii, the greatest difference in selectivity is observed between La^{3+} and all other metals. Similar preference for smaller ionic radii ions was demonstrated in the metal-mediated aggregation of the Lamp peptide[23] and other Ln^{3+} chelators,[17] corresponding to trends in Lewis acidity. Collectively, we hypothesize that multi-chain assembly is driven by hydrophobic moieties that offer an optimized configuration of ligands. Further, smaller pendant side chains are too small

to effectively drive intermolecular interactions and bulkier side chains interfere with efficient assembly (Figure 3d).

Mechanistic insights into metal binding-driven aggregation

With connections identified between copolymer composition and efficiency in metal extraction, we sought to elucidate the relationships between composition and solution structure driving the phase separation of metal-complexed copolymers. Towards this, we probed conformational changes induced by lanthanide binding using SEC_{aq} in the presence and absence of a representative lanthanide ion, Eu^{3+}. Chain compaction was observed for conformational ensembles of **P1-BA(5)**, as the presence of Eu^{3+} (0.1 mM Eu^{3+}, 40 mM MES, 100 mM KCl, pH 6) results in a smaller apparent $M_{p\ (PEG)}$ as compared analysis in a metal-free buffer (40 mM MES, 100 mM KCl, pH 6; Figure 4a, left). However, for the most hydrophobic copolymer, **P3-BA(15)**, both chain compaction and assembly (i.e., an additional peak at a higher $M_{p\ (PEG)}$) are observed (Figure 4a, right and Figure S35). Analysis of SEC_{aq} of copolymers with different hydrophobic side chains also demonstrates a predominant single-chain conformation in metal-free conditions, with the appearance of a more compact structure upon metal-binding for all copolymers with aggregation additional present for **P8-LA**, **P5-*c*HA**, and **P6-HA** (Figure S36). These data suggest that, in the dilute metal regime, metal chelation drives copolymers to adopt more compact structures before promoting aggregation.

To glean more insight into the conformational change occurring upon metal-binding, we additionally performed SAXS analysis on **P1-BA(5)**, **P5-*c*HA**, **P6-HA**, and **P8-LA** in the presence of metal ions. These copolymers span a range of hydrophobic alkyl side chain lengths and architectures and have also demonstrated differing metal extraction efficiency (Figure 3c), offering an interesting scope to unravel differences in compaction upon Eu^{3+} binding. Samples were incubated with Eu^{3+} at a ratio of $[Eu^{3+}]/[AA]= 0.1$ to minimize turbidity during the measurement. Due to some aggregation observed at polymer concentration of 5 mg/mL, measurements taken at 2.5 mg/mL were used to estimate R_g used to normalize the scattering intensity plots (Figure S37). Analysis of the scattering profiles in a dimensionless Kratky projection allows for comparisons across copolymers (2.5 mg/mL) with and without metal to reveal changes in polymer conformation due to metal binding (Figure 4b and SAF-AG, Table S1). In this projection, **P6-HA** demonstrates a large shift in the scattering profile highlighting a more compact structure upon the addition of metal as compared to **P5-*c*HA** and **P1-BA(5)** as demonstrated by a plateau at intermediate $q \bullet R_g$. The large conformational change conferred by metal binding to **P6-HA** correlates with the increase in efficacy of ion isolation; thus, we hypothesize this compaction may drive chain assembly and maximize metal isolation efficiency. Similar processes have also been demonstrated in intrinsically disordered proteins, where folding and liquid-liquid separation have been induced by metal binding.[60] For example, the metal binding drives local chain ordering and dimerization of the lanmodulin protein derived from *Hansschlegelia quercus*, contributing to this desirable property.[61] In contrast to these polymers, **P8-LA** is more structured compared to the other three polymers in

the absence of Eu^{3+}, as demonstrated by a Porod exponent of 2.2. However, metal chelation further confers even more of a compact morphology to the polymer with an increase in Porod to 3.1 (Figure 4b[iv]). However, we observe that this additional compaction does not offer increased ion extraction (Figure 3c). This behavior may resemble traditional metalloenzymes[62] or lanmodulin derived from *Methylobacterium extorquens,*[63] where metal-binding does not result in changes in quaternary structure required to promote assembly.

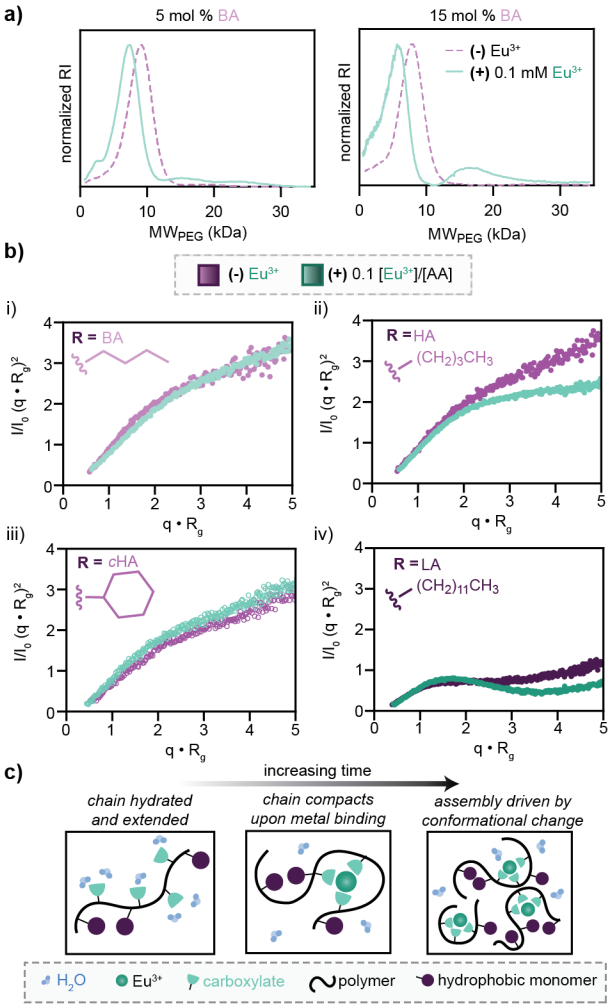

Figure 4. Mechanistic insights into metal binding-driven aggregation. (a) SEC_{aq} for 5 and 15 mol % butyl acrylate (BA) copolymers [**P1-BA(5)**] and 15 mol % [**P3-BA(15)**] in the presence and absence of Eu^{3+}. Molecular weights are determined by comparison to PEG calibrants. (b) Dimensionless Kratky projections of SAXS profiles before (purple) and after (green) incubation with Eu^{3+} for (i) butyl acrylate (BA) copolymer [**P1-BA(5)**], (ii) *n*-hexyl acrylate (HA) copolymer (**P6-HA**), (iii) cyclohexyl acrylate (*c*HA) copolymer (**P5-*c*HA)**, and (iv) lauryl acrylate (LA) copolymer (**P8-LA**). (c) Proposed binding-then-assembly mechanism for ion extraction using polymer precipitants.

From these data, we hypothesize three steps are involved in the metal-driven precipitation (Figure 4c). The unbound soluble chain begins in a relatively disordered conformation in part due to negatively charged AA groups (Figure 4a, b). Upon metal binding, the chain adopts a compacted conformation due to metal-mediated intramolecular crosslinking (Figure 4a). The elimination of solvated negative charges and the presence of hydrophobic side chains further drives compaction through the hydrophobic effect (Figure 4a, b[ii]). Aggregation of these chains is the final step, as poorly solvated chains form intermolecular interactions (Figure 4a, right). Maximizing metal pulldown is therefore both a function of effectively driving polymer folding through metal binding as well as the resulting chain conformation self-assembling into large aggregates. Similar examples of a binding event succeeded by multi-chain assembly formation have been described in metal-ligand coordinated supramolecular polymers[64] in addition to complexation of poly(amides) to anionic analytes.[65]

Impact of monomer patterning and sequence arrangement

To further explore the complex relationship between the thermoresponsive, structural, and functional copolymer components on the Ln^{3+} pulldown efficiency, we designed two multiblock copolymers (**b1** and **b2**). Monomer sequence patterning through multiblock copolymer synthesis of thermoresponsive NIPAM copolymers has been shown to broaden the temperature ranges of morphological transitions[66] and confer hysteresis in transmittance recovery during cooling.[67] We therefore hypothesized that multiblock copolymers would exhibit altered efficiency for the isolation of rare earth ions and allow mechanistic insights into the coprecipitation. To understand the effect of colocalizing the binding, thermoresponsive, and structural motifs, we synthesized the block copolymer p(NIPAM)-*b*-p(AA-*co*-BA)-*b*-p(NIPAM) (**b1**), where the thermoresponsive region is fully segregated from the binding and structural region. We also synthesized p(NIPAM-*co*-AA-*co*-BA)-*b*-p(NIPAM)-*b*-p(NIPAM-*co*-AA-*co*-BA) (**b2**) to probe effects enriching the local density of binding and structural motifs along the backbone. Finally, a separate statistical p(NIPAM-*co*-AA-*co*-BA) (**stat**) was prepared with a similar composition to **b1** and **b2** for comparison (Figure 5a).

Tri-block copolymers (**b1** and **b2**) were synthesized using RAFT polymerization with intermediate purification by preparative gel permeation chromatography between blocks. Samples were collected before and after polymerization for ^{1}H NMR and GPC analysis to determine the composition of each block (Tables S4-S8, Figures S38-45). The resulting copolymers were synthesized with approximately 25 mol % *t*BA and 10 mol % BA to target higher Ln^{3+} extraction efficiency and accommodate any decreases in efficiency conferred through monomer patterning. As with the statistical copolymers discussed above, the trithiocarbonate chain ends were capped and the AA units were revealed following the deprotection of *t*BA units in acid (Figures S46-48).

We found that the efficiency of Ln^{3+} ion isolation at 28 °C was strongly dependent on monomer patterning. Segregating the binding and structural units from the thermoresponsive region caused

b1 to perform significantly worse than **stat** across all ions tested (Figure 5b). However, the extraction efficiency of **b1** was improved to the level of **stat** by increasing the incubation temperature to 31 °C (Figure 5c, S49). These results suggest that proximity of the binding, structural and thermoresponsive monomers is required to efficiently insolubilize the polymer-ion complex at moderate temperatures. Structurally, **b1** displayed a broad peak at high molecular weights by SEC_{aq} in metal-free buffer conditions indicative of a multi-chain assembly driven by the dense hydrophobic center block that cannot rely on NIPAM monomers to facilitate improved solvation (Figure 5d). The aggregation of **b1** prior to binding may obstruct the diffusion of metal ions to binding sighs and reduce pulldown efficiency (Figure 5e).

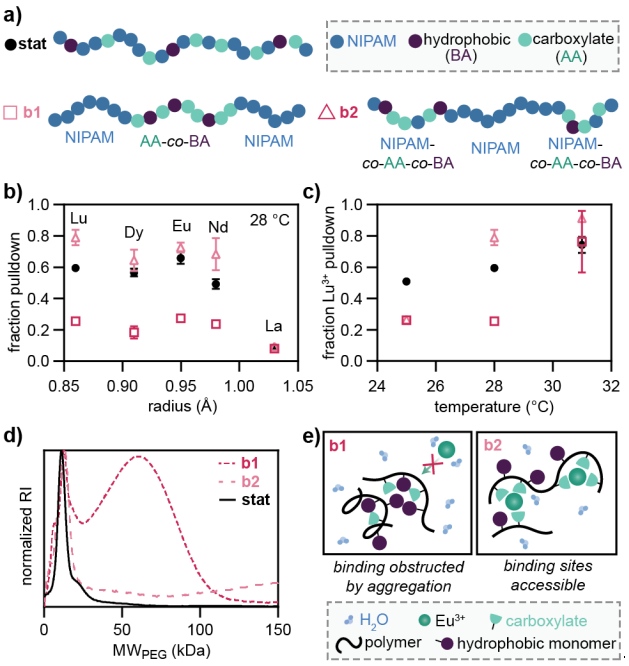

Figure 5. Evaluating the impact of monomer patterning on lanthanide separation. (a) Schematic illustrating the design of two sequence-controlled triblock copolymers (**b1**, **b2**) with the three-comonomer scope of N-isopropylacrylamide, NIPAM), butyl acrylate (BA), and acrylic acid (AA). A compositionally comparable statistical copolymer (**stat**) is also shown. (b) Relative efficiency of Ln^{3+} ion extraction (denoted in plot) by **b1**, **b2**, and **stat** copolymers at 28 °C (n = 3, error bars represent standard deviation). (c) Fraction of Lu^{3+} isolated by **b1**, **b2**, and **stat** copolymers at 25 °C, 28 °C, and 31 °C (n = 3, error bars represent standard deviation). (d) SEC_{aq} chromatograms of **b1**, **b2**, and **stat**. Molecular weights are determined from PEG calibration curve. (e) Schematic of two potential aggregation mechanisms for **b1** and **b2**.

In contrast, **b2** slightly outperforms or has very similar metal isolation efficiency to **stat** across most ionic radii at 28 °C. Compared to the large decrease in efficiency with removal of NIPAM

from the binding and structural region (as shown by **b1**), this modest increase in efficiency suggests the more subtle effects of local density of binding and structural units interspersed with NIPAM (Figure 5b, S49). However, similar to **b1**, increasing incubation temperature also increases the pulldown efficiency by conferring increased hydrophobicity to the thermoresponsive backbone (Figure 5c). By SEC_{aq}, **b2** resembles a single-chain, similar to **stat**, suggesting that distribution of NIPAM comonomers aids in chain solvation despite enrichment of the structural and binding at ends of the chain (Figure 5d). For both **b1** and **b2**, addition of 0.1 mM Eu^{3+} in the SEC_{aq} buffer shifts conformational ensembles to larger aggregates, consistent with previous observations (Figure S50). Therefore, carefully considering how structural and chelating elements are interspersed with thermoresponsive comonomers through sequence patterning offers another avenue to tune assembly mechanisms and ion extraction efficiency (Figure 5e).

Finally, monomer patterning was observed to modulate the temperature range necessary to improve efficiency of ion extraction (Figure S49). For example, the bound fraction of Lu^{3+} by **b1** was improved was improved from 0.25 to above 0.90 over a small temperature change of 6 °C, Comparatively, for **stat**, we observe a much smaller increase (from 0.50 to 0.70) in a similar temperature range. Block copolymerization results in sequence ensembles that are inherently enriched in certain polymer sequences as compared to their statistical copolymer counterparts. This increased colocalization between structural and binding units may drive efficient dehydration of the polymer complexed to Ln^{3+} and promote aggregation. Quantifying the relationship between block copolymer composition and their self-assembly through complex energy landscapes continues to be an area of active work, spanning simulation studies on the kinetics of nucleation and coalescence[68] to experimental efforts characterizing the impact of concentration, temperature, and sequence in solid-gel phase transitions.[69]

Conclusion

We here demonstrate composition-structure-function relationships in a model system of lanthanide (Ln) binding and precipitation. We have rationally designed and synthesized a suite of copolymers with a thermoresponsive backbone supplemented with binding and structural comonomers. Using a colorimetric dye assay, we have developed a workflow to quantitate relationships between copolymer composition and the pulldown efficacy towards different Ln^{3+} ions. We have systematically quantitated the ability of polymer hydrophobicity, monomer architecture, and monomer patterning to modulate the pulldown efficiency towards a variety of ionic radii in the lanthanide series. This analysis revealed the significance of the Van der Waals surface area of hydrophobic comonomers in driving metal isolation and the importance of local composition through sequence patterning in modulating assembly. Finally, we gleaned mechanistic insights into how the copolymer composition impacts the in-solution structure of the chain as well as metal-induced compaction.

A deeper understanding of composition-structure-function relationships in synthetic macromolecules offer potential applications as catalysts, chemical sequestrants, and even in encoding information. This work represents one step in a broader effort towards elucidating relevant design principles in disordered materials to facilitate their *de novo* design. Further work in these directions includes the study of architecture effects (e.g., branching, cross-linking, and stars) in modulating selectivity and affinity towards different lanthanides as well as probing sequence effects through gradient and multiblock copolymers. These materials begin to bridge the gap towards embedding protein-mimetic functionality into synthetic macromolecules, a critical step in the design of materials with complex functionality.

Acknowledgements

This material is supported by the U.S. Department of Energy, Office of Science, Office of Basic Energy Sciences under Award Number DE-SC0021295. S.S.C. acknowledges support from the National Science Foundation Graduate Research Fellowship Program under award number DGE-204035. We thank the UNC NMR Core Laboratory supported by NSF award number CHE-1828183 and the Zhukhovitskiy group for their assistance with preparative gel permeation chromatography. This work was conducted in part at the Advanced Light Source at Lawrence Berkeley National Laboratory on behalf of the Department of Energy, Office of Basic Energy Sciences, through the Integrated Diffraction Analysis Technologies (IDAT) program, supported by DOE Office of Biological and Environmental Research, the National Institute of Health project ALS-ENABLE (P30 GM124169), and a High-End Instrumentation Grant S10OD018483. This material has benefitted from the use of SasView software, originally developed under NSF award DMR-0520547 and also supported by funding from the European Union's Horizon 2020 research and innovation program under the SINE2020 project, grant agreement number 654000. We are grateful to Dr. Gregory Hura at Lawrence Berkeley National Laboratory for SAXS data collection and valuable insights, and the Longleaf cluster supported by the UNC Computing Cluster for providing computational support and resources.

References

(1) Zhao, G.; Huang, X.; Tang, Z.; Huang, Q.; Niu, F.; Wang, X. Polymer-Based Nanocomposites for Heavy Metal Ions Removal from Aqueous Solution: A Review. *Polym. Chem.* **2018**, *9* (26), 3562–3582. https://doi.org/10.1039/C8PY00484F.

(2) Mann, J. L.; Maikawa, C. L.; Smith, A. A. A.; Grosskopf, A. K.; Baker, S. W.; Roth, G. A.; Meis, C. M.; Gale, E. C.; Liong, C. S.; Correa, S.; Chan, D.; Stapleton, L. M.; Yu, A. C.; Muir, B.; Howard, S.; Postma, A.; Appel, E. A. An Ultrafast Insulin Formulation Enabled by High-Throughput Screening of Engineered Polymeric Excipients. *Sci. Transl. Med.* **2020**, *12*, 1–12.

(3) DeStefano, A. J.; Segalman, R. A.; Davidson, E. C. Where Biology and Traditional Polymers Meet: The Potential of Associating Sequence-Defined Polymers for Materials Science. *JACS Au* **2021**, *1* (10), 1556–1571. https://doi.org/10.1021/jacsau.1c00297.

(4) Tan, X.; Sawczyk, M.; Chang, Y.; Wang, Y.; Usman, A.; Fu, C.; Král, P.; Peng, H.; Zhang, C.; Whittaker, A. K. Revealing the Molecular-Level Interactions between Cationic Fluorinated Polymer Sorbents and the Major PFAS Pollutant PFOA. *Macromolecules* **2022**, *55* (3), 1077–1087. https://doi.org/10.1021/acs.macromol.1c02435.
(5) Wijker, S.; Palmans, A. R. A. Protein-Inspired Control over Synthetic Polymer Folding for Structured Functional Nanoparticles in Water. *ChemPlusChem* **2023**, *88* (7), e202300260. https://doi.org/10.1002/cplu.202300260.
(6) Mundsinger, K.; Izuagbe, A.; Tuten, B. T.; Roesky, P. W.; Barner-Kowollik, C. Single Chain Nanoparticles in Catalysis. *Angew. Chem. Int. Ed.* **2023**, e202311734. https://doi.org/10.1002/anie.202311734.
(7) Sanders, M. A.; Chittari, S. S.; Sherman, N.; Foley, J. R.; Knight, A. S. Versatile Triphenylphosphine-Containing Polymeric Catalysts and Elucidation of Structure–Function Relationships. *J. Am. Chem. Soc.* **2023**, *145* (17), 9686–9692. https://doi.org/10.1021/jacs.3c01092.
(8) Dignon, G. L.; Zheng, W.; Kim, Y. C.; Mittal, J. Temperature-Controlled Liquid–Liquid Phase Separation of Disordered Proteins. *ACS Cent. Sci.* **2019**, *5* (5), 821–830. https://doi.org/10.1021/acscentsci.9b00102.
(9) Lorenzo, R. A.; Carro, A. M.; Concheiro, A.; Alvarez-Lorenzo, C. Stimuli-Responsive Materials in Analytical Separation. *Anal. Bioanal. Chem.* **2015**, *407* (17), 4927–4948. https://doi.org/10.1007/s00216-015-8679-1.
(10) Lu, H.; Wang, Y.; Li, L.; Kotsuchibashi, Y.; Narain, R.; Zeng, H. Temperature- and pH-Responsive Benzoboroxole-Based Polymers for Flocculation and Enhanced Dewatering of Fine Particle Suspensions. *ACS Appl. Mater. Interfaces* **2015**, *7* (49), 27176–27187. https://doi.org/10.1021/acsami.5b09874.
(11) O'Shea, J.-P.; Qiao, G. G.; Franks, G. V. Temperature Responsive Flocculation and Solid–Liquid Separations with Charged Random Copolymers of Poly(*N*-Isopropyl Acrylamide). *J. Colloid Interface Sci.* **2011**, *360* (1), 61–70. https://doi.org/10.1016/j.jcis.2011.04.013.
(12) Onogi, S.; Lee, S.-H.; Fruehauf, K. R.; Shea, K. J. Abiotic Stimuli-Responsive Protein Affinity Reagent for IgG. *Biomacromolecules* **2021**, *22* (6), 2641–2648. https://doi.org/10.1021/acs.biomac.1c00335.
(13) Mittal, V.; Matsko, N. B.; Butté, A.; Morbidelli, M. Swelling Deswelling Behavior of PS-PNIPAAM Copolymer Particles and PNIPAAM Brushes Grafted from Polystyrene Particles & Monoliths. *Macromol. Mater. Eng.* **2008**, *293* (6), 491–502. https://doi.org/10.1002/mame.200700409.
(14) Huang, T.; Su, Z.; Hou, K.; Zeng, J.; Zhou, H.; Zhang, L.; P. Nunes, S. Advanced Stimuli-Responsive Membranes for Smart Separation. *Chem. Soc. Rev.* **2023**, *52* (13), 4173–4207. https://doi.org/10.1039/D2CS00911K.
(15) Yamashita, K.; Nishimura, T.; Ohashi, K.; Ohkouchi, H.; Nango, M. Two-Step Imprinting Procedure of Inter-Penetrating Polymer Network-Type Stimuli-Responsive Hydrogel-Adsorbents. *Polym. J.* **2003**, *35* (7), 545–550. https://doi.org/10.1295/polymj.35.545.
(16) Dong, R.; Li, J.; Xiong, H.; Lu, W.; Peng, H.; Chen, L. Thermosensitive Molecularly Imprinted Polymers on Porous Carriers: Preparation, Characterization and Properties as Novel Adsorbents for Bisphenol A. *Talanta* **2014**, *130*, 182–191. https://doi.org/10.1016/j.talanta.2014.06.055.
(17) Cheisson, T.; Schelter, E. J. Rare Earth Elements: Mendeleev's Bane, Modern Marvels. *Science* **2019**, *363* (6426), 489–493. https://doi.org/10.1126/science.aau7628.

(18) Deblonde, G. J.-P.; Chagnes, A.; Cote, G. Recent Advances in the Chemistry of Hydrometallurgical Methods. *Sep. Purif. Rev.* **2023**, *52* (3), 221–241. https://doi.org/10.1080/15422119.2022.2088389.
(19) Xie, F.; Zhang, T. A.; Dreisinger, D.; Doyle, F. A Critical Review on Solvent Extraction of Rare Earths from Aqueous Solutions. *Miner. Eng.* **2014**, *56*, 10–28. https://doi.org/10.1016/j.mineng.2013.10.021.
(20) Felipe, E. C. B.; Batista, K. A.; Ladeira, A. C. Q. Recovery of Rare Earth Elements from Acid Mine Drainage by Ion Exchange. *Environ. Technol.* **2021**, *42* (17), 2721–2732. https://doi.org/10.1080/09593330.2020.1713219.
(21) Qi, X.-H.; Du, K.-Z.; Feng, M.-L.; Gao, Y.-J.; Huang, X.-Y.; Kanatzidis, M. G. Layered A2Sn3S7·1.25H2O (A = Organic Cation) as Efficient Ion-Exchanger for Rare Earth Element Recovery. *J. Am. Chem. Soc.* **2017**, *139* (12), 4314–4317. https://doi.org/10.1021/jacs.7b00565.
(22) A. Mattocks, J.; A. Cotruvo, J. Biological, Biomolecular, and Bio-Inspired Strategies for Detection, Extraction, and Separations of Lanthanides and Actinides. *Chem. Soc. Rev.* **2020**, *49* (22), 8315–8334. https://doi.org/10.1039/D0CS00653J.
(23) Hatanaka, T.; Matsugami, A.; Nonaka, T.; Takagi, H.; Hayashi, F.; Tani, T.; Ishida, N. Rationally Designed Mineralization for Selective Recovery of the Rare Earth Elements. *Nat. Commun.* **2017**, *8* (1), 15670. https://doi.org/10.1038/ncomms15670.
(24) Archer, W. R.; Gallagher, C. M. B.; Vaissier Welborn, V.; Schulz, M. D. Exploring the Role of Polymer Hydrophobicity in Polymer-Metal Binding Thermodynamics. *Phys. Chem. Chem. Phys.* **2022**, *24* (6), 3579–3585. https://doi.org/10.1039/d1cp05263b.
(25) Archer, W. R.; Chen, T.; Vaissier Welborn, V.; Schulz, M. D. Polymer Tacticity Effects in Polymer–Lanthanide Chelation Thermodynamics. *Macromolecules* **2023**, *56* (22), 9062–9069. https://doi.org/10.1021/acs.macromol.3c01163.
(26) Dykeman-Bermingham, P. A.; Bogen, M. P.; Chittari, S. S.; Grizzard, S. F.; Knight, A. S. Tailoring Hierarchical Structure and Rare Earth Affinity of Compositionally Identical Polymers via Sequence Control. *J. Am. Chem. Soc.* **2024**, *146* (12), 8607–8617. https://doi.org/10.1021/jacs.4c00440.
(27) Zhang, Q.; Vancoillie, G.; Mees, M. A.; Hoogenboom, R. Thermoresponsive Polymeric Temperature Sensors with Broad Sensing Regimes. *Polym. Chem.* **2015**, *6* (13), 2396–2400. https://doi.org/10.1039/C4PY01747A.
(28) Xu, X.; Bizmark, N.; Christie, K. S. S.; Datta, S. S.; Ren, Z. J.; Priestley, R. D. Thermoresponsive Polymers for Water Treatment and Collection. *Macromolecules* **2022**, *55* (6), 1894–1909. https://doi.org/10.1021/acs.macromol.1c01502.
(29) Lutz, J.-F.; Akdemir, Ö.; Hoth, A. Point by Point Comparison of Two Thermosensitive Polymers Exhibiting a Similar LCST: Is the Age of Poly(NIPAM) Over? *J. Am. Chem. Soc.* **2006**, *128* (40), 13046–13047. https://doi.org/10.1021/ja065324n.
(30) Li, B.; Thompson, M. E. Phase Transition in Amphiphilic Poly(N-Isopropylacrylamide): Controlled Gelation. *Phys. Chem. Chem. Phys.* **2018**, *20* (19), 13623–13631. https://doi.org/10.1039/C8CP01609G.
(31) Lv, C.; Zhang, Z.; Gao, J.; Xue, J.; Li, J.; Nie, J.; Xu, J.; Du, B. Self-Assembly of Thermosensitive Amphiphilic Pentablock Terpolymer PNIPAMx-b-PtBA90-b-PPO36-b-PtBA90-b-PNIPAMx in Dilute Aqueous Solution. *Macromolecules* **2018**, *51* (24), 10136–10149. https://doi.org/10.1021/acs.macromol.8b01933.

(32) Ramírez-Irigoyen, A. J.; García-Verdugo, K. F.; Castillo-Ortega, M. M.; Rodríguez-Félix, D. E.; Encinas, J. C.; Plascencia-Jatomea, M.; Argüelles-Monal, W.; Sauceda, I. S.; Pérez-González, R.; del Castillo-Castro, T. Study of Thermal Transitions of Copolymers Based on N-Isopropylacrylamide and Acrylic Acid with Potential for Curcumin Controlled Release. *J. Appl. Polym. Sci.* **2023**, *140* (35), e54338. https://doi.org/10.1002/app.54338.
(33) Shieh, Y.-T.; Lin, P.-Y.; Chen, T.; Kuo, S.-W. Temperature-, pH- and CO2-Sensitive Poly(N-Isopropylacryl Amide-Co-Acrylic Acid) Copolymers with High Glass Transition Temperatures. *Polymers* **2016**, *8* (12), 434. https://doi.org/10.3390/polym8120434.
(34) Bokias, G.; Staikos, G.; Iliopoulos, I. Solution Properties and Phase Behaviour of Copolymers of Acrylic Acid with *N*-Isopropylacrylamide: The Importance of the Intrachain Hydrogen Bonding. *Polymer* **2000**, *41* (20), 7399–7405. https://doi.org/10.1016/S0032-3861(00)00090-2.
(35) Cheng, J.; Shan, G.; Pan, P. Triple Stimuli-Responsive N-Isopropylacrylamide Copolymer toward Metal Ion Recognition and Adsorption via a Thermally Induced Sol–Gel Transition. *Ind. Eng. Chem. Res.* **2017**, *56* (5), 1223–1232. https://doi.org/10.1021/acs.iecr.6b03626.
(36) Ju, X.-J.; Zhang, S.-B.; Zhou, M.-Y.; Xie, R.; Yang, L.; Chu, L.-Y. Novel Heavy-Metal Adsorption Material: Ion-Recognition P(NIPAM-Co-BCAm) Hydrogels for Removal of Lead(II) Ions. *J. Hazard. Mater.* **2009**, *167* (1), 114–118. https://doi.org/10.1016/j.jhazmat.2008.12.089.
(37) Mizoguchi, K.; Ida, J.; Matsuyama, T.; Yamamoto, H. Straight-Chained Thermo-Responsive Polymer with High Chelating Group Content for Heavy Metal Ion Recovery. *Sep. Purif. Technol.* **2010**, *75* (1), 69–75. https://doi.org/10.1016/j.seppur.2010.07.013.
(38) Sakai, R.; Matsuyama, T.; Ida, J. Effect of Immobilization Method and Particle Size on Heavy Metal Ion Recovery of Thermoresponsive Polymer/Magnetic Particle Composites. *Colloids Surf. Physicochem. Eng. Asp.* **2020**, *590*, 124499. https://doi.org/10.1016/j.colsurfa.2020.124499.
(39) Tomonaga, H.; Tanigaki, Y.; Hayashi, K.; Matsuyama, T.; Ida, J. Adsorption Properties of Poly(NIPAM-Co-AA) Immobilized on Silica-Coated Magnetite Nanoparticles Prepared with Different Acrylic Acid Content for Various Heavy Metal Ions. *Chem. Eng. Res. Des.* **2021**, *171*, 213–224. https://doi.org/10.1016/j.cherd.2021.05.005.
(40) Plummer, R.; Hill, D. J. T.; Whittaker, A. K. Solution Properties of Star and Linear Poly(N-Isopropylacrylamide). *Macromolecules* **2006**, *39* (24), 8379–8388. https://doi.org/10.1021/ma0614545.
(41) Sze Ieong, N.; Hasan, M.; J. Phillips, D.; Saaka, Y.; K. O'Reilly, R.; I. Gibson, M. Polymers with Molecular Weight Dependent LCSTs Are Essential for Cooperative Behaviour. *Polym. Chem.* **2012**, *3* (3), 794–799. https://doi.org/10.1039/C2PY00604A.
(42) Filippov, A. D.; Van Hees, I. A.; Fokkink, R.; Voets, I. K.; Kamperman, M. Rapid and Quantitative De- Tert-Butylation for Poly(Acrylic Acid) Block Copolymers and Influence on Relaxation of Thermoassociated Transient Networks. *Macromolecules* **2018**, *51* (20), 8316–8323. https://doi.org/10.1021/acs.macromol.8b01440.
(43) Du, J.; Willcock, H.; Patterson, J. P.; Portman, I.; O'Reilly, R. K. Self-Assembly of Hydrophilic Homopolymers: A Matter of RAFT End Groups. *Small* **2011**, *7* (14), 2070–2080. https://doi.org/10.1002/smll.201100382.
(44) Mondal, T.; Ghosh, S. A Remarkable Impact of a Minor Structural Variation in the Chain-End on the Hierarchical Self-Assembly of a Polymeric Foldamer. *Polym. Chem.* **2016**, *7* (44), 6735–6743. https://doi.org/10.1039/C6PY01486K.

(45) Moad, G.; Rizzardo, E.; Thang, S. H. End-Functional Polymers, Thiocarbonylthio Group Removal/Transformation and Reversible Addition-Fragmentation-Chain Transfer (RAFT) Polymerization: Thiocarbonylthio Group Removal/Transformation. *Polym. Int.* **2011**, *60* (1), 9–25. https://doi.org/10.1002/pi.2988.
(46) Chen, P.; Chen, J.; Cao, Y. Self-Assembly Behavior of Thermo- and Ph-Responsive Diblock Copolymer of Poly(N-Isopropylacrylamide)- Block-Poly(Acrylic Acid) Synthesized Via Reversible Addition-Fragmentation Chain Transfer Polymerization. *J. Macromol. Sci. Part A* **2013**, *50* (5), 478–486. https://doi.org/10.1080/10601325.2013.780947.
(47) Heskins, M.; Guillet, J. E. Solution Properties of Poly(N-Isopropylacrylamide). *J. Macromol. Sci. Part - Chem.* **1968**, *2* (8), 1441–1455. https://doi.org/10.1080/10601326808051910.
(48) Hogendoorn, C.; Roszczenko-Jasińska, P.; Martinez-Gomez, N. C.; de Graaff, J.; Grassl, P.; Pol, A.; Op den Camp, H. J. M.; Daumann, L. J. Facile Arsenazo III-Based Assay for Monitoring Rare Earth Element Depletion from Cultivation Media for Methanotrophic and Methylotrophic Bacteria. *Appl. Environ. Microbiol.* **2018**, *84* (8), e02887-17. https://doi.org/10.1128/AEM.02887-17.
(49) Gumfekar, S. P.; Soares, J. B. P. Polymer Reaction Engineering Tools to Design Multifunctional Polymer Flocculants. *Chemosphere* **2018**, *210*, 156–165. https://doi.org/10.1016/j.chemosphere.2018.06.175.
(50) Qi, X.; Wang, Z.; Ma, S.; Wu, L.; Yang, S.; Xu, J. Complexation Behavior of Poly(Acrylic Acid) and Lanthanide Ions. *Polymer* **2014**, *55* (5), 1183–1189. https://doi.org/10.1016/j.polymer.2014.01.051.
(51) Hazra, A.; Ghosh, C.; Banerjee, F.; Samanta, S. K. Highly Efficient Main-Chain Cationic Polyelectrolytes for Selective Sensing of Permanganate, Perrhenate, and Heparin. *ACS Appl. Polym. Mater.* **2024**, *6* (11), 6540–6551. https://doi.org/10.1021/acsapm.4c00805.
(52) Hammouda, B. SANS from Homogeneous Polymer Mixtures: A Unified Overview. In *Polymer Characteristics*; Advances in Polymer Science; Springer: Berlin, Heidelberg, 1993; pp 87–133. https://doi.org/10.1007/BFb0025862.
(53) Hammouda, B. A New Guinier–Porod Model. *J. Appl. Crystallogr.* **2010**, *43* (4), 716–719. https://doi.org/10.1107/S0021889810015773.
(54) Kachala, M.; Valentini, E.; Svergun, D. I. Application of SAXS for the Structural Characterization of IDPs. In *Intrinsically Disordered Proteins Studied by NMR Spectroscopy*; Felli, I. C., Pierattelli, R., Eds.; Springer International Publishing: Cham, 2015; pp 261–289. https://doi.org/10.1007/978-3-319-20164-1_8.
(55) Brethomé, A. V.; Fletcher, S. P.; Paton, R. S. Conformational Effects on Physical-Organic Descriptors: The Case of Sterimol Steric Parameters. *ACS Catal.* **2019**, *9* (3), 2313–2323. https://doi.org/10.1021/acscatal.8b04043.
(56) Caldeweyher, E.; Bauer, C.; Tehrani, A. S. An Open-Source Framework for Fast-yet-Accurate Calculation of Quantum Mechanical Features. *Phys. Chem. Chem. Phys.* **2022**, *24* (17), 10599–10610. https://doi.org/10.1039/D2CP01165D.
(57) Terashima, T.; Sugita, T.; Fukae, K.; Sawamoto, M. Synthesis and Single-Chain Folding of Amphiphilic Random Copolymers in Water. *Macromolecules* **2014**, *47* (2), 589–600. https://doi.org/10.1021/ma402355v.
(58) Warren, J. L.; Dykeman-Bermingham, P. A.; Knight, A. S. Controlling Amphiphilic Polymer Folding beyond the Primary Structure with Protein-Mimetic Di(Phenylalanine). *J. Am. Chem. Soc.* **2021**, *143* (33), 13228–13234. https://doi.org/10.1021/JACS.1C05659.

(59) Neal, T. J.; Parnell, A. J.; King, S. M.; Beattie, D. L.; Murray, M. W.; Williams, N. S. J.; Emmett, S. N.; Armes, S. P.; Spain, S. G.; Mykhaylyk, O. O. Control of Particle Size in the Self-Assembly of Amphiphilic Statistical Copolymers. *Macromolecules* **2021**, *54* (3), 1425–1440. https://doi.org/10.1021/acs.macromol.0c02341.
(60) Mukhopadhyay, S. The Dynamism of Intrinsically Disordered Proteins: Binding-Induced Folding, Amyloid Formation, and Phase Separation. *J. Phys. Chem. B* **2020**, *124* (51), 11541–11560. https://doi.org/10.1021/acs.jpcb.0c07598.
(61) Mattocks, J. A.; Jung, J. J.; Lin, C.-Y.; Dong, Z.; Yennawar, N. H.; Featherston, E. R.; Kang-Yun, C. S.; Hamilton, T. A.; Park, D. M.; Boal, A. K.; Cotruvo, J. A. Enhanced Rare-Earth Separation with a Metal-Sensitive Lanmodulin Dimer. *Nature* **2023**, *618* (7963), 87–93. https://doi.org/10.1038/s41586-023-05945-5.
(62) Valdez, C. E.; Smith, Q. A.; Nechay, M. R.; Alexandrova, A. N. Mysteries of Metals in Metalloenzymes. *Acc. Chem. Res.* **2014**, *47* (10), 3110–3117. https://doi.org/10.1021/ar500227u.
(63) Cotruvo, J. A.; Featherston, E. R.; Mattocks, J. A.; Ho, J. V.; Laremore, T. N. Lanmodulin: A Highly Selective Lanthanide-Binding Protein from a Lanthanide-Utilizing Bacterium. *J. Am. Chem. Soc.* **2018**, *140* (44), 15056–15061. https://doi.org/10.1021/jacs.8b09842.
(64) Gröger, G.; Meyer-Zaika, W.; Böttcher, C.; Gröhn, F.; Ruthard, C.; Schmuck, C. Switchable Supramolecular Polymers from the Self-Assembly of a Small Monomer with Two Orthogonal Binding Interactions. *J. Am. Chem. Soc.* **2011**, *133* (23), 8961–8971. https://doi.org/10.1021/ja200941a.
(65) Rostami, A.; Wei, C. J.; Guérin, G.; Taylor, M. S. Anion Detection by a Fluorescent Poly(Squaramide): Self-Assembly of Anion-Binding Sites by Polymer Aggregation. *Angew. Chem. Int. Ed.* **2011**, *50* (9), 2059–2062. https://doi.org/10.1002/anie.201006884.
(66) Farias-Mancilla, B.; Balestri, A.; Zhang, J.; Frielinghaus, H.; Berti, D.; Montis, C.; Destarac, M.; Schubert, U. S.; Guerrero-Sanchez, C.; Harrisson, S.; Lonetti, B. Morphology and Thermal Transitions of Self-Assembled NIPAM-DMA Copolymers in Aqueous Media Depend on Copolymer Composition Profile. *J. Colloid Interface Sci.* **2024**, *662*, 99–108. https://doi.org/10.1016/j.jcis.2024.02.032.
(67) Ohnsorg, M. L.; Ting, J. M.; Jones, S. D.; Jung, S.; Bates, F. S.; Reineke, T. M. Tuning PNIPAm Self-Assembly and Thermoresponse: Roles of Hydrophobic End-Groups and Hydrophilic Comonomer. *Polym. Chem.* **2019**, *10* (25), 3469–3479. https://doi.org/10.1039/C9PY00180H.
(68) Lam, Y.-M.; Goldbeck-Wood, G. Mesoscale Simulation of Block Copolymers in Aqueous Solution: Parameterisation, Micelle Growth Kinetics and the Effect of Temperature and Concentration Morphology. *Polymer* **2003**, *44* (12), 3593–3605. https://doi.org/10.1016/S0032-3861(03)00250-7.
(69) Cui, S.; Yu, L.; Ding, J. Thermogelling of Amphiphilic Block Copolymers in Water: ABA Type versus AB or BAB Type. *Macromolecules* **2019**, *52* (10), 3697–3715. https://doi.org/10.1021/acs.macromol.9b00534.